Energy Transport in High-Density Spin-Exchange Optical Pumping Cells

D. K. Walter, W. M. Griffith, and W. Happer
Department of Physics, Princeton University, Princeton, New Jersey 08544
(Received 15 December 2000)

We present *in situ* measurements of temperatures inside multi-atmosphere spin-exchange optical pumping cells using Raman scattering from the N_2 quenching gas. Under conditions usually prevailing in spin-exchange optical pumping experiments, we find that gas temperatures can be elevated hundreds of degrees above ambient, and that convection plays a very important role in the heat transport of the system.

DOI: 10.1103/PhysRevLett.86.3264 PACS numbers: 33.20.Fb, 32.80.Bx, 44.25.+f

The technologies of optical pumping [1] and spin-exchange optical pumping [2] have in recent years pervaded diverse areas of research, having been employed in the search for fundamental symmetries [3], the enhancement of biological magnetic resonance imaging [4], and the study of the spin structure of the neutron [5], to name but a few. In the attempt to produce ever-larger quantities of noble gas with high ($\gtrsim$0.5) polarizations, increasingly intense sources of pump radiation have been used, evolving from the milliwatt alkali discharge lamps of the earliest experiments [6,7], through several-watt Ti:sapphire lasers [8,9], to the 100-W (or more) diode laser arrays used in much current work [10]. As a result, typically tens of watts of absorbed optical energy are converted to thermal energy in a volume of a few deciliters, leading to substantial temperature gradients which drive heat flow out of the pump chamber. While much effort has been expended in understanding the flow of angular momentum in optical pumping systems [11,12], the concomitant flow of energy is poorly understood, although important for several reasons: (1) Some key rates of angular momentum transfer exhibit a very strong temperature dependence; for example, the Rb spin-destruction rate due to helium scales as $\sim T^{4.3}$ [12]. (2) The heating of the pump chamber in two-chambered polarized target cells of e^--scattering experiments causes difficult-to-quantify density changes in the target chamber, which can be the dominant systematic error of the measured absolute cross sections [13]. (3) As shown by the experiments below, the widely held assumption that heat (and noble-gas nuclear spin polarization) is transported by diffusion to the cell walls is incorrect. Under practical conditions of spin-exchange optical pumping to produce large quantities of hyperpolarized ^{3}He or ^{129}Xe, convection is more important than diffusion.

In this Letter we present the results of an experimental investigation of energy transport *in situ* in high-density optical pumping cells of the variety currently used in practical systems. Using the Raman scattering of a probe beam from the N_2 buffer gas in the pumping cell, we measure the vibrational and rotational temperatures of the nitrogen, from which we are able to infer the local (translational) temperature of the buffer gas with 1-mm spatial resolution. With this technique we demonstrate the existence of convection in spin-exchange optical pumping cells under ordinary operating conditions and quantify the absolute temperature of the gas in the pump chamber.

In the first step of the optical pumping of an alkali-metal atom, a circularly polarized D_1 photon is absorbed by the ground state atom. In order to suppress reradiation of the excited-state atom—which will degrade the desired polarization induced by the pump beam, as the accompanying photon is unpolarized, isotropically emitted, and resonant—enough N_2 buffer gas (usually 60–100 torr) is added to the system to deexcite a large fraction (0.95–0.99) of the excited alkali atoms via radiationless, two-body quenching collisions [14], in which the diatomic molecule absorbs into its internal degrees of freedom the $\sim$1.5 eV of the D_1 transition. As a result, the optical energy absorbed by the alkali vapor is converted almost completely into heat. Immediately following a quenching collision, the N_2 molecule occupies a highly excited ($v = 5, 6$) vibrational state; this energy is thermalized in subsequent equilibrating collisions with neighboring buffer-gas atoms. The three important time scales of the process are the vibrational-vibrational *equilibration* time $\tau_{\text{V-V}}$, the vibrational-to-rotational/translational *relaxation* time $\tau_{\text{V-R/T}}$, and the rotational-to-translational relaxation time $\tau_{\text{R-T}}$. While the vibrational relaxation times can be extremely long due to the large vibrational frequencies of the nitrogen (discussed below), the rotational relaxation is effected in only a few collisions [15], and $\tau_{\text{R-T}} \sim 1$ ns: It is therefore possible that the vibrational temperature T_{vib} of the nitrogen be elevated with respect to the rotational and translational temperatures T_{rot} and T_{tr}, but to an excellent approximation $T_{\text{rot}} = T_{\text{tr}}$, whence the local rotational temperature of the nitrogen is a good measure of the local bulk temperature of the gas. Although easily measured by a temperature sensor affixed to the glass, the temperature of the pump-chamber wall depends on the amount of laser absorption by the glass and can vary greatly over the surface of the cell, making it a poor indicator of the internal gas temperature.

The rotational temperatures can be measured by observing the well-known Raman scattering of an intense beam from the molecular nitrogen [16]. The inelastically Raman-scattered photons of the primary beam connect rotational

 0031-9007/01/86(15)/3264(4)$15.00

states of the nitrogen with $\Delta J = \pm 2$. The number of photons scattering from state J into state J' per unit time from a volume V of nitrogen (number density $[N_2]$) illuminated by a primary beam of intensity I is [17]

$$\Gamma_{J\to J'} = IV[N_2] g_J (2J + 1) \frac{e^{-E_J/kT_{\rm rot}}}{Z} \sigma_{J\to J'}, \quad (1)$$

where g_J is the statistical factor arising from the identical-boson exchange symmetry requirements of the nitrogen nuclei, $E_J = J(J + 1)hcB_0$ is the rotational energy of the initial state, and Z is the rotational partition function. The cross section $\sigma_{J\to J'}$, which contains the J-dependent Placzek-Teller matrix element [18] and scales with the cube of the Raman frequency, is on the order of 10^{-30} cm^2. The faint scattered light is thus a probe of the populations of the nitrogen rotational states, from which the rotational temperature $T_{\rm rot}$ can be extracted.

A diagram of the apparatus is shown in Fig. 1. A flowing-air oven containing the Pyrex [19] optical pumping cell is situated in a field of ~6 G produced by a pair of Helmholtz coils; the oven temperature is maintained with a feedback loop at $T_{\rm amb}$. The rubidium vapor is pumped by a high-power, 2-nm-wide (FWHM) fiber-coupled diode laser array at the wavelength of the Rb D_1 transition. A power meter at the exit face of the oven monitors the transmitted pump intensity, from which the power deposited in the cell can be deduced. In order to vary over a wide range the amount of power absorbed by the vapor at a fixed oven temperature, the polarization of the pump beam can be switched between circular and linear, its intensity attenuated with neutral density filters, or its center wavelength detuned by changing the laser current. The 6-W Raman primary beam, furnished by the 5145-Å line of an argon-ion laser, enters the cell from above and can be focused to a narrow waist at nearly any point inside the cell with a position resolution of 1 mm. The probe beam is imaged with a planoconvex lens onto the entrance slit of a Spex 1404 double Raman spectrometer (with 0.85-m focal length), at the exit slit of which is mounted a bi-alkali photomultiplier tube configured for photon counting. A personal computer uses a data acquisition board to control the spectrometer grating-rotation motor and to count the logic pulses generated by the discriminator. The raw data thus consist of a set of photon counts as a function of wavelength.

A representative rotational Raman scan is presented in Fig. 2. Each individual scan, spanning at least 16 well-resolved peaks of the rotational spectrum, was taken by counting photons for a fixed dwell time at wavelength intervals of 0.08 Å. Typically, scans were repeated to increase the signal-to-noise ratio. The analysis is carried out by first fitting each peak to a Gaussian of three parameters (amplitude, width, baseline) to obtain the total peak count and its relative error. This set of error-weighted peak heights is then fit to Eq. (1), with three parameters: an overall scale factor, a linear baseline, and the temperature. Errors in the temperature measurement depended on the total photon count, ranging from less than 1% for pure N_2 cells to several percent for cells containing small nitrogen concentrations.

An important result of this work is the observation of convective heat transfer in the optical pumping cell. Figure 3 shows the temperature measured at a fixed point near the front center of a 40-cm^3 cell, containing 2.0 amg ^{4}He [20] and 0.33 amg N_2, as a function of power deposited in the cell, for $T_{\rm amb} = 170$ °C. The measured gas temperature increases linearly with the absorbed power to a point, at which it begins to deviate from the line, with the deviation becoming greater as the power is further increased. For purely conductive heat transfer, the temperature rise is expected to be linear in the power deposited, with slope α/k, where α is a factor depending only on the cell

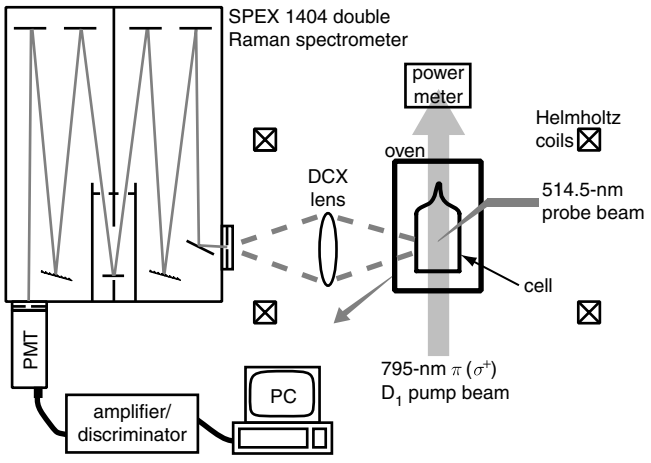

FIG. 1. Block diagram of the experimental apparatus. The D_1 pump source is furnished by a fiber-coupled diode laser array, the probe beam by the 514.5-nm line of a 15-W water-cooled argon-ion laser.

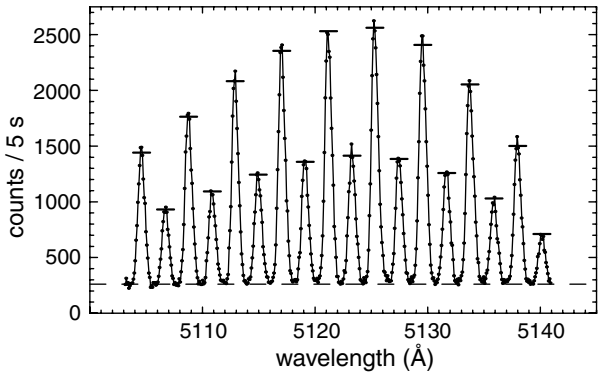

FIG. 2. Representative rotational Raman scan, taken on a 2.0 amg He + 0.33 amg N_2 mixture. The dwell time for each scan (repeated 5 times) was 1 sec; the step size was 0.08 Å. The solid line connects the data points, shown as dots. The horizontal bars show the results of a fit to Eq. (1) with constant baseline (dashed line), yielding a temperature of 363 °C.

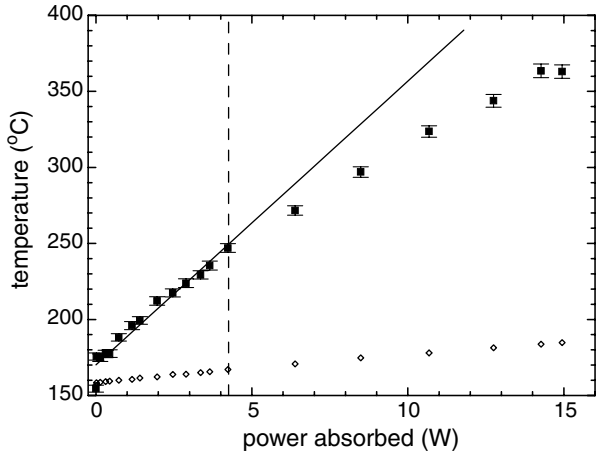

FIG. 3. Dependence on absorbed power of gas temperature (squares) at a fixed point in the center of a 40-cm^3 cell containing 2.0 amg He and 0.33 amg N_2, in an oven maintained at 170 °C. The line is a fit to the data points up to 4.3 W absorbed power, beyond which the measured temperature rise deviates increasingly from the linear dependence expected in a purely conductive model. The temperature at a point on the side cell wall measured by a sensor attached to the glass is also shown (diamonds).

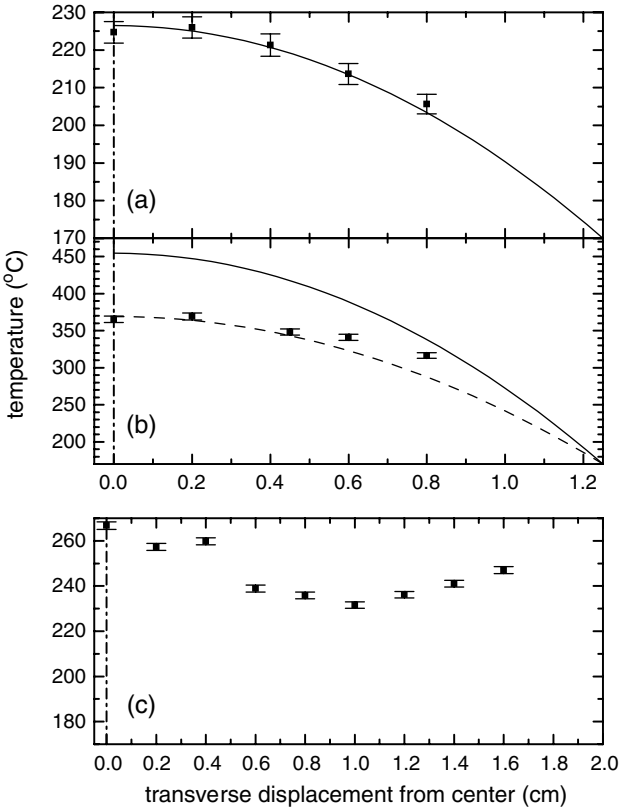

FIG. 4. Measured gas temperatures (squares) transverse to the pump axis: (a) 2.9 W absorbed and (b) 15 W absorbed in the cell of Fig. 3, and (c) 10 W absorbed in a 100-cm^3 cell containing 1.5 amg N_2. The broken vertical line indicates the axis of symmetry of the cell. The solid curve in (a) is a parabola fit to the data, a function which is an excellent approximation of the solution to the 3D diffusion equation with constant source term. The solid curve in (b) is the curve of (a) scaled by the ratio of the absorbed powers. The dashed curve in (b), an attempt to fit the data to a parabola, illustrates the flattening of the profile.

geometry and k is the thermal conductivity. Consideration of the dimensionless Rayleigh number—the ratio of the buoyant to the viscous forces in the fluid—helps to interpret these data. The Rayleigh number $\mathcal{R}$ of a gas with coefficient of thermal expansion β, kinematic viscosity ν, and thermal diffusivity χ is given by $\mathcal{R} = \beta g \Theta h^3/\nu\chi$, where g is the acceleration due to gravity, Θ the characteristic temperature rise of the gas, and h is a characteristic length, which we take to be half the vertical height of the cell. For a given geometry there exists a critical Rayleigh number $\mathcal{R}_{cr}$ at which the fluid becomes unstable against small density perturbations and begins to convect; for $\mathcal{R} < \mathcal{R}_{cr}$, convection is absent, and heat flows via conduction. As $\mathcal{R}$ increases above $\mathcal{R}_{cr}$, convection develops more fully. From the onset of convection inferred from Fig. 3, we find $\mathcal{R}_{cr} \approx 1400$. In comparison, for the simple and related case of two infinite parallel plates held at different temperatures, theory shows that $\mathcal{R}_{cr} = 1708$ [21].

The difference between conductive and convective heat transfer modes can be clearly seen in spatial profiles of the temperature distribution transverse to the pump beam propagation axis. Figure 4 shows the temperature variations across the cell of Fig. 3 for the cases of both low and high power absorption. For the data of Fig. 4(a), the Rayleigh number is 1300, less than $\mathcal{R}_{cr}$; in Fig. 4(b), $\mathcal{R} = 2500$, greater than $\mathcal{R}_{cr}$, where convection is present. The flattening out and lowering of the temperatures away from the walls in the second case is a signature of convective heat transfer, for which most of the temperature drop occurs in a thin boundary layer at the wall. At even larger $\mathcal{R}$ it is likely that higher-order convection modes occur; Fig. 4(c) shows a profile consistent with such an interpretation. Here a cell (containing 1.5 amg N_2) 4 cm $\times$ 4 cm in cross section was illuminated only in its center, in a circular region 2.5 cm in diameter. The local minimum in the temperature profile coincides with the boundary between two convective cells.

The magnitudes of the absolute temperature rise of the buffer gas in spin-exchange optical pumping cells are also striking. For example, in a cylindrical, 75-cm^3 pump chamber filled with 3 amg of an 89% ^{4}He/10% N_2/1% Xe mixture—commonly used in flowing Xe-polarization devices—we observe at the center of the cell a 105 °C elevation of the gas temperature above the oven temperature when 15 W of pump light is absorbed in the cell. Likewise, in the spherical 100-cm^3 pump chamber of a two-chambered 185-cm^3 cell containing 8.4 amg ^{3}He and 50 torr N_2, a configuration often used in the target cells of nuclear scattering experiments [5], we measure an elevation of 95 °C for 22 W deposited in the cell. A summary of data taken on several different cells is shown in Table I.

TABLE I. Measured slopes of temperature vs absorbed power and Rayleigh numbers for cells included in our study. A range of slopes is shown where the data indicate curvature, e.g., as seen in Fig. 3. Where no range of slopes is given, it is only for the high power range of 5–15 W. The Rayleigh number is computed for a 50 °C rise for that gas mixture and geometry, using h = one-half the cell height, and thermal conductivities k from Refs. [25] and [26]. The elevated vibrational temperatures in the cases of pure N_2 imply a larger heat capacity, but were not considered in the calculation.

Contents (amg)	Cell[a]	Slope (K/W)	k [W/(m · K)]	$\mathcal{R}$
1.0 He + 0.33 N_2	*A*	14	0.14	400
2.0 He + 0.33 N_2	*A*	11–19	0.17	700
	B	10		1300
	C	6		3000
3.0 He + 0.16 N_2	*A*	7	0.20	750
1.5 N_2	*A*	13	0.039	7000
	C	8–15		30 000
3.2 N_2	*A*	6		28 000
	D	5		800 000

[a]Cells are square-faced box shapes with face widths, volumes: (*A*) 25 mm, 40 cm^3; (*B*) 30 mm, 60 cm^3; (*C*) 40 mm, 100 cm^3; with the exception of cell type *D*, which is a 220 cm^3 spherical cell.

Since the interatomic potential of molecular nitrogen is very nearly harmonic for the lowest-lying vibrational states of interest in these experiments (and therefore the energy differences between adjacent vibrational states are very nearly equal), the process of vibrational excitation transfer in collisions between nitrogen molecules is extremely efficient, to the extent that even under conditions of intense pumping, the distribution of the nitrogen among its vibrational levels is governed by a Boltzmann distribution with a vibrational temperature T_{vib} [22,23]. Despite the difficulties caused by the small occupation numbers of the excited vibrational states and the unfortunate accidental coincidences of a few vibrational Raman lines of nitrogen with some weak argon-ion lines, we have been able to measure vibrational temperatures.

Measurements of the anti-Stokes (blue) N_2 vibrational Raman lines in a cell containing 3.2 amg of N_2 alone indicate an extremely high temperature of approximately 900 °C at 16 W of absorption. That this temperature is elevated above the rotational temperature is a consequence of the slow relaxation of vibrational modes to rotational/translational modes of the gas [22]. In contrast, the vibrational temperature of a (3 amg He + 0.33 amg N_2) cell is found to be very roughly the rotational temperature (elevated 120 °C above ambient) at 15 W of absorption, in accord with the fact that the N_2 vibrational to He translational relaxation time is much shorter than $\tau_{\mathrm{V\text{-}R/T}}$ for N_2-N_2 [23]. While it is expected that the N_2 vibrational temperatures would be elevated as one substitutes a heavier buffer gas, in most current incarnations of optical pumping an abundance of helium is present. The topic of energy transport may need to be revisited, however, when high-power diode lasers are developed with sufficiently narrow spectral width [24] to efficiently optically pump Rb for spin-exchange polarization of ^{129}Xe with little or no additional helium.

D. K. W. is supported by the Hertz Foundation. This work was supported by the AFOSR and NSF.

[1] W. Happer, Rev. Mod. Phys. **44**, 169 (1972).
[2] T. G. Walker and W. Happer, Rev. Mod. Phys. **69**, 629 (1997).
[3] R. E. Stoner, M. A. Rosenberry, J. T. Wright, T. E. Chupp, E. R. Oteiza, and R. L. Walsworth, Phys. Rev. Lett. **77**, 3971 (1996).
[4] M. S. Albert, G. D. Cates, B. Driehuys, W. Happer, B. Saam, C. S. Springer, Jr., and A. Wishnia, Nature (London) **370**, 199 (1994).
[5] K. Abe *et al.,* Phys. Rev. Lett. **79**, 26 (1997).
[6] A. Kastler, J. Opt. Soc. Am. **47**, 460 (1957).
[7] M. A. Bouchiat, T. R. Carver, and C. M. Varnum, Phys. Rev. Lett. **5**, 373 (1960).
[8] P. L. Anthony *et al.,* Phys. Rev. Lett. **71**, 959 (1993).
[9] H. Middleton *et al.,* Magn. Reson. Med. **33**, 271 (1995).
[10] B. Driehuys, G. D. Cates, E. Miron, K. Sauer, D. K. Walter, and W. Happer, Appl. Phys. Lett. **69**, 1668 (1996).
[11] C. J. Erickson *et al.,* Phys. Rev. Lett. **85**, 4237 (2000).
[12] A. Ben-Amar Baranga *et al.,* Phys. Rev. Lett. **80**, 2801 (1998).
[13] I. Kominis (private communication).
[14] P. L. Bender, Ph.D. thesis, Princeton University, 1956; E. S. Hrycyshyn and L. Krause, Can. J. Phys. **48**, 2761 (1970).
[15] D. R. Miller and R. P. Andres, J. Chem. Phys. **46**, 3418 (1967); A. E. Belikov, R. G. Sharafutdinov, and A. V. Storozhev, Chem. Phys. **213**, 319 (1996).
[16] A. Compaan, A. Wagoner, and A. Aydinli, Am. J. Phys. **62**, 639 (1994).
[17] C. M. Penney, R. L. St. Peters, and M. Lapp, J. Opt. Soc. Am. **64**, 712 (1974).
[18] G. Placzek and E. Teller, Z. Phys. **81**, 209 (1932).
[19] In the course of our experiments we discovered that the intense argon-ion probe beam readily bores holes through some types of aluminosilicate glass. We surmise that this phenomenon is due to thermal runaway of the temperature-dependent photon absorption of Fe sites in iron-rich glass.
[20] One amagat (amg) equals 2.689×10^{19} cm^{-3}, the number density of an ideal gas at 273 K and 1 atmosphere.
[21] L. D. Landau and E. M. Lifshitz, *Fluid Mechanics* (Pergamon, Oxford, 1987).
[22] E. Weitz and G. Flynn, Annu. Rev. Phys. Chem. **25**, 275 (1974).
[23] L. Y. Nelson, A. W. Saunders, Jr., A. B. Harvey, and G. O. Neely, J. Chem. Phys. **55**, 5127 (1971).
[24] B. Chann, I. Nelson, and T. G. Walker, Opt. Lett. **25**, 1352 (2000).
[25] J. Kestin, S. T. Ro, and W. A. Wakeham, J. Chem. Phys. **56**, 4036 (1972).
[26] R. D. Fleeter, J. Kestin, R. Paul, and W. A. Wakeham, Physica (Amsterdam) **108A**, 371 (1981).